Results in Engineering 6 (2020) 100104

Contents lists available at ScienceDirect

Results in Engineering

journal homepage: www.editorialmanager.com/rineng/Default.aspx

# Qualitatively-improved identified parameters of prestressed concrete catenary poles using sensitivity-based Bayesian approach

F. Alkam [a,*], I. Pereira [b], T. Lahmer [a,**]

[a] Institute of Structural Mechanics (ISM), Bauhaus-Universität Weimar, 99423, Germany
[b] Department of Mathematics, CIDMA, University of Aveiro, Portugal

ARTICLE INFO

*Keywords:*
Prestressed concrete catenary poles
Bayesian inference
Inverse problems
Sensitivity analysis
TMCMC
Vibration test
3-Point bending test

ABSTRACT

Prestressed, spun-cast ultrahigh-strength concrete catenary poles have been used widely for electric train systems; for example, thousands of these poles have been installed along high-speed train tracks in Germany. Given the importance of the functionality of train systems, adequate attention has not been paid to catenary poles in research and the literature. Questions regarding the integrity of catenary poles still exist. This study contributes to identify the actual material properties of the poles of interest because the parameter identification is an essential process for any subsequent evaluation of the integrity of catenary poles. Accordingly, a sensitivity-based Bayesian parameter identification approach is developed to estimate the real material properties of the poles using measurements from multiple experiments and numerical models. This approach integrates the sensitivity of time-dependent measurements into the Bayesian inference, which improves the quality of inferred parameters considerably in comparison with classic Bayesian approaches applied in similar case of studies. Furthermore, the proposed approach combines observations of multiple experiments conducted on full-scale poles using a probabilistic uncertainty framework, which provides informative data used in the parameter identification process. Besides, Bayesian inference quantifies the uncertainty of inferred parameters and estimates the hyperparameters, such as the total errors of the observations. The proposed approach utilizes the efficiency of the transitional Markov Chain Monte Carlo algorithm for sampling from the posterior in both levels of Bayesian inference, namely, the unknown parameters and the hyperparameters. The results show the significant influence of the sensitivity concept in improving the quality of the posterior and highlight the importance of identifying the real material properties during the evaluation of the behavior of existing structures, rather than using the characteristic properties from the datasheet. Applying the proposed approach looks very promising when applied to similar applied case studies.

## 1. Introduction

Poles are used worldwide to support power transmission, telephone and telegraph lines, street lighting, antenna masts, and overhead power lines for electric trains. For many years, poles were made of wood, steel, and concrete. In the early years of the 20$^{th}$ century, concrete poles were made of normal reinforced concrete [1]. The quality of concrete poles increased rapidly by developing some techniques, such as prestressed concrete, spun-cast methods, and advanced curing processes [2]. This improves the durability of the poles, making them lighter and stronger, able to withstand more cyclic loads and increasing their resistance to environmental conditions [3,4]. Compared to steel poles, the prestressed, spun-cast concrete poles become more feasible, cheaper, have a longer operational life, and lower lifetime costs [5]. *Catenary poles* are structural members that suspend the catenary systems of electric trains. Prestressed, spun-cast catenary poles made from ultrahigh-strength concrete have been widely used in the electric train systems. For example, thousands of this type of poles have been installed in Germany along new high-speed train tracks, reaching a speed of 330km h$^{-1}$.

Given their importance to the functionality of the entire train system, scant attention has been paid to the behavior of the catenary poles in the literature, especially for those supporting train systems. Researches were mainly focused on the train-induced vibration and their effects on the catenary system and surroundings without paying adequate attention to

* Corresponding author.
** Corresponding author.
*E-mail addresses:* feras.alkam@uni-weimar.de (F. Alkam), isabel.pereira@ua.pt (I. Pereira), tom.lahmer@uni-weimar.de (T. Lahmer).

https://doi.org/10.1016/j.rineng.2020.100104
Received 28 November 2019; Received in revised form 11 February 2020; Accepted 12 February 2020

catenary poles. These are included (but are not limited to) the verification of train-induced ground vibrations [6,7], the interaction of train-induced vibration with surrounding soil and nearby structures [8], the collapse of noise protection walls along high-speed trains tracks [9], and the interaction of the pantograph of train and the catenary cables [10–12]. Therefore, questions about their integrity are still open.

A research project has built to track the behavior of the hollow section, spun-cast, prestressed ultrahigh-strength concrete catenary poles that are used in the high-speed electric train systems. The behavior of the poles under various actions (namely, static, environmental, and dynamic actions) is studied, considering the long-term changes in the material of the pole [13,14]. This project has been divided into three phases. In the first phase, which is the focus of this paper, actual material properties are identified, using measurements conducted on full-scale poles. In the second phase, data extracted from a Structural Health Monitoring (SHM) system installed on three poles along the train track, is analyzed. The third phase covers the future status and damage detection over the life of the poles.

*Parameter estimation* as a statistical term, or *Parameter Identification (PI)* as an engineering term, is currently one of the essential tasks of engineering and science, especially with the increasing capacity of computers that makes it more practical and efficient [15]. In engineering science, the PI process is generally associated with Uncertainty Quantification (UQ) frameworks solving ill-posed inverse problems due to imperfection of models, parameter uncertainty, and noisy measurements [16,17]. Moreover, the sensitivity of the parameters plays a vital role in finding solutions to inverse problems. The sensitivity makes the solution unstable, as a small change in the inputs can lead to a significant change in the estimated model parameters [18]. Two UQ frameworks are commonly used for identifying the parameters of systems, namely, the deterministic and the probabilistic approaches.

The deterministic solution of inverse problems uses the least-squares approach by minimizing the residuals between observations and model prediction. Regularization techniques (for example, Tikhonov regularization), can efficiently deal with the ill-posedness of inverse problems by adding the prior knowledge of the input parameters [19]. In deterministic UQ frameworks, the covariance matrix represents parameters uncertainties by estimating the local sensitivity of parameters at the optimal point, or the so-called Markov estimator [20,21].

The probabilistic UQ framework has two concepts, namely, the Frequentist and Bayesian concepts. The Frequentist concept uses the information contained in the sample, where observations are considered in terms of probability density functions, and the parameters can be estimated by least squares or Maximum Likelihood Estimators (MLEs) [22]. The Bayesian Inference combines two kinds of information: the prior information given by the parameter with the information contained in data; specifically, combines the prior probabilities of parameters with the probabilities of observations, conditional on given parameter values. The output is deduced in terms of probability distributions of the specified parameters, which makes it easy to quantify uncertainties by calculating the statistical properties of these distributions [15]. Bayesian inference is utilized to solve inverse problems efficiently [23]. One of the main challenges of using the Bayesian approach is extracting the information from the posterior density. Sampling methods are considered feasible alternatives to evaluate the posterior rather than the analytical integration. Most efficient sampling methods depend on Markov chain Monte Carlo (MCMC) methods [24].

As mentioned, this paper covers the first phase of the research project and has mainly two goals. First, identifying the actual material properties of the poles to use them later in evaluating the behavior of the poles and analyzing data obtained from the SHM system. Second, providing a sensitivity-based Bayesian approach that improves the quality of identified parameters by solving the problem caused by the low sensitivity of the likelihood with respect to some parameters during the PI process. This distinguishes this case study from other classic PI problems and increases its complexity; however, it is an additional motivation to adapt the classic Bayesian approach to achieve the desired objectives.

In the proposed approach, measurements of multiple experimental tests and results models done using the Finite Element Method (FEM) are conjugated. The results show the efficiency of considering the sensitivity of measurements on the quality of inferred parameters. Moreover, the results highlight the importance of using actual material properties rather than using characteristic values provided by manufacturers in the datasheet.

In Section 2, a detailed overview of Bayesian inference, and how it can be adapted to cover the aim of the current study, is provided. This is followed by the proposed solution in Section 3. The solution is built in two strategies that show both classical and proposed Bayesian approaches. The case study is presented in Section 4. The application is illustrated in Section 5 and followed by results and discussion in Section 6.

## 2. Methodology

### 2.1. Forward model

In this study, three types of parameters are considered: input parameters subjected to uncertainty $\boldsymbol{x} \in \mathscr{X} \subseteq \mathbb{R}^m$, non-physical input parameters $\boldsymbol{\xi} \in \mathscr{Z}$, and well-known deterministic input parameters, $\boldsymbol{d} \in \mathscr{D}$. In addition, hyperparameters $\boldsymbol{\theta} \in \Theta$ are sometimes needed to describe the vague uncertainty of parameters.

The outputs of the predictive model are $\boldsymbol{y} \in \mathscr{Y}$ with an output space $\mathscr{Y} \subseteq \mathbb{R}^n$. In engineering applications, $\boldsymbol{y}$ represents the *'real'* observations of the given system, which practically cannot be measured due to the uncertainty of the experimental models. It is more convenient to use the measured observation $\tilde{\boldsymbol{y}} \in \tilde{\mathscr{Y}} \subseteq \mathbb{R}^n$, such as, $\tilde{\boldsymbol{y}} = \boldsymbol{y} + \boldsymbol{\eta}$. The total prediction error $\boldsymbol{\eta}$ considers the discrepancy between the model prediction and the real system, and discrepancy between the response of the real system and measurands [25].

Using a *forward operator* $\mathscr{G}$, the mapping from the input parameters $\boldsymbol{x}$ to the measured outputs $\tilde{\boldsymbol{y}}$ defines the *forward model* $\mathscr{M}$, such that

$$\mathscr{M} : \mathscr{X} \times \mathscr{Z} \times \mathscr{D} \to \tilde{\mathscr{Y}} \qquad (\boldsymbol{x}, \boldsymbol{\xi}, \boldsymbol{d}) \mapsto \tilde{\boldsymbol{y}} = \mathscr{G}(\boldsymbol{x}, \boldsymbol{\xi}, \boldsymbol{d}) + \boldsymbol{\eta}\,. \tag{1}$$

### 2.2. Inverse problems

In many engineering applications, the observations of the system $\tilde{\boldsymbol{y}} \subseteq \mathbb{R}^n$ can be measured without knowing their inputs $\boldsymbol{x} \subseteq \mathbb{R}^m$. In this case, given the forward operator $\mathscr{G}$ and the observations $\tilde{\boldsymbol{y}}$, the inputs to be inferred are such that Eq. (1) holds. This type of *inverse problem* is referred to by engineers as a PI process [15]. The problem is considered as a *well-posed* problem if it fulfills the triple: existence, uniqueness, and stability. Practically, inverse problems are *ill-posed* as they mostly suffer from one or more of the three-mentioned causes [26]. Solving inverse problems becomes harder due to imperfection of the model, uncertainties, and noisy measurements [22]. Different techniques overcome the difficulties, for example, by utilizing informative priors, or so-called regularization techniques in the deterministic framework. In the probabilistic frameworks, the Bayesian inference is effectively used.

### 2.3. Bayesian inverse problems

The Bayesian approach, as a probabilistic framework of the UQ, overcomes the difficulties of solving inverse problems by considering the stochastic model of Eq. (1) such that $\tilde{\boldsymbol{Y}} = \mathscr{G}(\boldsymbol{X}, \boldsymbol{\xi}, \boldsymbol{d}) + \mathbf{E}$ [18], which is achieved by considering the observations as random variable $\tilde{\boldsymbol{Y}} = \{\tilde{Y}_1, \cdots, \tilde{Y}_n\}^T \in \mathbb{R}^n$, which has the probability distribution $\mathbf{P}_{\tilde{Y}}$ with a PDF $\pi(\tilde{\boldsymbol{y}}) > 0$. $\tilde{\boldsymbol{Y}}$ represents the multiple outputs of the given case study. Their realizations $\tilde{\boldsymbol{y}} = \{\tilde{y}_1, \cdots, \tilde{y}_n\}^T$ are observed directly from measurements.

The unknown parameter $\boldsymbol{X} = \{X_1, \cdots, X_m\}^T \in \mathbb{R}^m$ is a random variable

with a prior density $\pi_X(\boldsymbol{x}) = \pi_0(\boldsymbol{x})$. The error $\mathbf{E} \in \mathbb{R}^n$ is a random variable that is mutually independent of $\boldsymbol{X}$ and has a probability distribution $\mathbf{P}_\mathrm{E}$ with an appropriate density $\pi_\mathrm{E}(\boldsymbol{\eta})$ [27]. Based on Bayes' Theorem, the posterior probability distribution of $\boldsymbol{X}$ given the observed data $\tilde{\boldsymbol{Y}}$ is written such that

$$\pi(\boldsymbol{x}|\tilde{\boldsymbol{y}}) = \frac{\pi(\tilde{\boldsymbol{y}}|\boldsymbol{x}) \cdot \pi_0(\boldsymbol{x})}{\pi(\tilde{\boldsymbol{y}})} \,. \tag{2}$$

Thus, Eq. (2) shows the four-pillars for solving inverse problems in the Bayesian approach: the *posterior* $\pi(\boldsymbol{x}|\tilde{\boldsymbol{y}})$, the *likelihood* $\pi(\tilde{\boldsymbol{y}}|\boldsymbol{x})$, the *evidence* $\pi(\tilde{\boldsymbol{y}})$, and the *prior* $\pi_0(\boldsymbol{x})$ [28].

The prior density $\pi_0(\boldsymbol{x})$ represents any available knowledge of the system before the data are collected. This can be retrieved from similar systems or prior experience [29]. Nevertheless, the prior can be built into a hierarchical model based on the observed data. In this case, unknown parameters $\boldsymbol{x}$ are modeled conditionally on unknown *hyperparameters* $\boldsymbol{\theta}_X$. These hyperparameters are considered as random variables $\boldsymbol{\Theta}_X$ with prior density distributions $\boldsymbol{\Theta}_X \widetilde{\pi_{\boldsymbol{\Theta}_X}}(\boldsymbol{\theta}_X)$. This makes the prior, such that $\pi_0(\boldsymbol{x};\boldsymbol{\theta}_X)$ and increases the number of inferred parameters [30].

However, it is common to consider the observations $\tilde{\boldsymbol{Y}}$ and hyperparameters of the inputs $\boldsymbol{\Theta}_X$ as mutually independent, that is, $\pi(\tilde{\boldsymbol{y}}|\boldsymbol{x}, \boldsymbol{\theta}_X) = \pi(\tilde{\boldsymbol{y}}|\boldsymbol{x})$. Thus, the stochastic forward model is updated such that $\tilde{\boldsymbol{Y}} = \mathscr{G}(\boldsymbol{X}, \boldsymbol{\Theta}_X, \boldsymbol{\xi}, \boldsymbol{d}) + \mathbf{E}$. In most cases, input parameters are conditionally independent, then the prior of the unknown parameters are evaluated from $\pi(\boldsymbol{x};\boldsymbol{\theta}_X) = \prod_{i=1}^{m} \pi(x_i|\boldsymbol{\theta}_X)$.

In some case studies, the realizations $\boldsymbol{\eta} = \{\eta_1, \cdots, \eta_n\}^T$ of the total errors $\mathbf{E}$ are not well-known (for example, because they are not quantified through experiments). By this, additional hyperparameters $\boldsymbol{\theta}_\mathrm{E}$ with a prior distribution $\pi_{\boldsymbol{\Theta}_\mathrm{E}}(\boldsymbol{\theta}_\mathrm{E})$ are added to unknown parameters. $\boldsymbol{\theta}_\mathrm{E}$ is needed to define the density distribution of the error $\mathbf{E}\widetilde{\pi_\mathrm{E}}(\boldsymbol{\eta};\boldsymbol{\theta}_\mathrm{E})$. Assuming that $\boldsymbol{\theta}_\mathrm{E}$ is mutually independent of $\boldsymbol{x}$ and $\boldsymbol{\theta}_X$, the joint prior distribution is written, as follows:

$$\pi_0(\boldsymbol{x}, \boldsymbol{\theta}_X, \boldsymbol{\theta}_\mathrm{E}) = \left(\prod_{i=1}^{m} \pi(x_i|\boldsymbol{\theta}_X)\right) \cdot \pi_{\boldsymbol{\Theta}_X}(\boldsymbol{\theta}_X) \cdot \pi_{\boldsymbol{\Theta}_\mathrm{E}}(\boldsymbol{\theta}_\mathrm{E}) \,. \tag{3}$$

The likelihood $\pi(\tilde{\boldsymbol{y}}|\boldsymbol{x})$ in Eq. (2) is a function of $\boldsymbol{y}$ with $\boldsymbol{x}$ fixed. To evaluate this, the Bayesian inference utilizes the concept of MLE from the Frequentist approach. This means that the specifications of the likelihood are based on the error model, which leads to $\pi(\tilde{\boldsymbol{y}}|\boldsymbol{x}) := \pi(\tilde{\boldsymbol{y}} - \mathscr{G}(\boldsymbol{x},\boldsymbol{\xi},\boldsymbol{d}))$, in other words $\mathscr{L}(\boldsymbol{x}, \boldsymbol{\xi}, \boldsymbol{d}|\tilde{\boldsymbol{y}}, \boldsymbol{\theta}_\mathrm{E})$, where $\mathscr{L}$ is the likelihood function [31]. Assuming random variables $\mathbf{E}$ to be independent and identically distributed (iid), the likelihood function [23] is estimated, as follows:

$$\pi(\tilde{\boldsymbol{y}}|\boldsymbol{x}) \equiv \mathscr{L}(\boldsymbol{x}, \boldsymbol{\xi}, \boldsymbol{d}|\tilde{\boldsymbol{y}}, \boldsymbol{\theta}_\mathrm{E}) = \prod_{i=1}^{m} \pi_\mathrm{E}(\tilde{y}_i - \mathscr{G}_i(\boldsymbol{x}, \boldsymbol{\xi}, \boldsymbol{d}); \Sigma_{ii}) \,, \tag{4}$$

with $\Sigma_{ii}$ being the $i^{th}$ component of the main diagonal of matrix $\boldsymbol{\Sigma}$. Accordingly, the posterior in Eq. (2) is described as follows:

$$\pi(\boldsymbol{x}, \boldsymbol{\theta}_X, \boldsymbol{\theta}_\mathrm{E}|\tilde{\boldsymbol{y}}) = \frac{\pi(\tilde{\boldsymbol{y}}|\boldsymbol{x}) \cdot \pi_0(\boldsymbol{x}, \boldsymbol{\theta}_X, \boldsymbol{\theta}_\mathrm{E})}{\pi(\tilde{\boldsymbol{y}})} \,. \tag{5}$$

The denominator of Eq. (5), the so-called evidence, is independent of $\boldsymbol{x}$ and represents the probability density of $\tilde{\boldsymbol{y}}$ for all values of $\boldsymbol{x}$. Hence, it is considered as a normalization constant and evaluated by the integral over all the possible joint densities of $\tilde{\boldsymbol{y}}$ such as

$$z = \pi(\tilde{\boldsymbol{y}}) = \int_{\mathscr{X}} \int_{\mathscr{Z}} \int_{\Theta_X} \int_{\Theta_\mathrm{E}} \mathscr{L}(\boldsymbol{x}, \boldsymbol{\xi}, \boldsymbol{d}|\tilde{\boldsymbol{y}}, \boldsymbol{\theta}_\mathrm{E})\, \pi_0(\boldsymbol{x}, \boldsymbol{\theta}_X, \boldsymbol{\theta}_\mathrm{E})\, \mathrm{d}\boldsymbol{x}\, \mathrm{d}\boldsymbol{\xi}\, \mathrm{d}\boldsymbol{\theta}_X \mathrm{d}\boldsymbol{\theta}_\mathrm{E} \,. \tag{6}$$

As a result, the posterior in Eq. (5) is written as a statement of proportionality, such as $\pi(\boldsymbol{x}, \boldsymbol{\theta}_X, \boldsymbol{\theta}_\mathrm{E}|\tilde{\boldsymbol{y}}) \propto \pi(\tilde{\boldsymbol{y}}|\boldsymbol{x}) \cdot \pi_0(\boldsymbol{x}, \boldsymbol{\theta}_X, \boldsymbol{\theta}_\mathrm{E})$.

Finally, the posterior density $\pi(\boldsymbol{x}|\tilde{\boldsymbol{y}})$ is a probability distribution that provides the full information of the unknown parameters $\boldsymbol{x}$, based on the observations $\boldsymbol{y}$. In some case studies, the interest is only in estimating the statistical moments, for example, the mean and the variance, as Quantity of Interests (QoIs). Here, keep in mind that the normalization constant $z$ should be included to have the right values of QoIs. In other cases, the *maximum a posteriori* (MAP) estimator $\widehat{\boldsymbol{x}}^{MAP}$, or *mode* as statistically named, is estimated. Thus, MAP represents the values of inferred parameters with the highest probabilities of occurrence, without the need to calculate the normalization factor $z$ [32], such that

$$\widehat{\boldsymbol{x}}^{MAP} = \underset{\boldsymbol{x} \in \mathbb{R}^m}{\operatorname{argmax}}\ \pi(\boldsymbol{x}|\tilde{\boldsymbol{y}}) \,. \tag{7}$$

One of the challenges of the Bayesian approach is extracting information from the posterior. Any parameter can be inferred directly through the marginalization of the posterior over the rest of the parameters such as $\pi(x_i|\tilde{\boldsymbol{y}}) = \int \pi(\boldsymbol{x}|\tilde{\boldsymbol{y}})\, \mathrm{d}\boldsymbol{x}_{\sim i}$, where $\boldsymbol{x}_{\sim i} = (x_1, \cdots, x_{i-1}, x_{i+1}, \cdots, x_m)$ denotes the parameters except $x_i$. In most cases, this cannot be solved analytically without using other simplification methods, such as asymptotic approximation [33], or by using stochastic sampling such that MC integration, and importance sampling [34]. Practically, MCMC algorithms are used for drawing the parameter distributions from the posterior, even those that are complex and high-dimensional [24].

### 2.4. Markov chain Monte Carlo

The MCMC method combines the Markov chain and MC integration for constructing chains whose stationary distribution is the posterior. The densities of parameters based on the observations are the realizations of the Markov chain [32,35]. Many different MCMC algorithms have been developed over in recent years. Most are mainly based on the probability of proposing the future state, for example, Metropolis-Hastings (MH), Gibbs sampling, and Slice sampling [36,37].

Among MCMC algorithms, the Transitional Markov chain Monte Carlo (TMCMC) is a widely used algorithm for solving both levels of the Bayesian inference, for example, parameter identification, model selection, and model averaging problems [38]. Because of its high efficiency, it is popular in engineering practice and inspiring in the research field [39,40]. The TMCMC algorithm overcomes many of the MH drawbacks, such as, stationary distribution of the chain, jumping step, correlation of accepted samples, and convergence of the chain [41–43]. Compared to the standard MH algorithm, drawn posterior density using TMCMC has better quality with a smaller number of samples [44]. Besides, TMCMC is suitable for sampling from multiple models, estimating the evidence of the Bayesian model class. It also overcomes the difficulty of sampling from complex models [45]. These reasons offer motivation to utilize the TMCMC algorithm in this study.

## 3. Proposed approach

The primary goal of the proposed approach is to improve the quality of inferred parameters. In this sense, the available observations of the conducted experiments are utilized and managed in two strategies to reach the target, as shown in Fig. 1. After implementing the proposed strategies, the quality of the results is compared. Then, the results with the best quality from one of the applied strategies are selected.

### 3.1. Strategy 1 (S1)

In this *All-in-one* strategy (S1), the observations of different experiments, or even the observations of different sensors in the same experiment, are formed in one observations vector $\tilde{\boldsymbol{Y}} = \{\tilde{\boldsymbol{Y}}^1, \cdots, \tilde{\boldsymbol{Y}}^K\}^T$ that has the corresponding models $\mathscr{M} = \{\mathscr{M}^1, \cdots, \mathscr{M}^K\}^T$. $K$ represents the number of conducted experiments, where the observations of the $k^{th}$ experiment are $\tilde{\boldsymbol{Y}}^k = \{\tilde{Y}_1^k, \cdots, \tilde{Y}_{n^k}^k\}^T$. The realizations of these random variables are $\tilde{\boldsymbol{y}}^k = \{\tilde{y}_1^k, \cdots, \tilde{y}_{n^k}^k\}^T \in \mathbb{R}^{n^k}$.

The global likelihood becomes

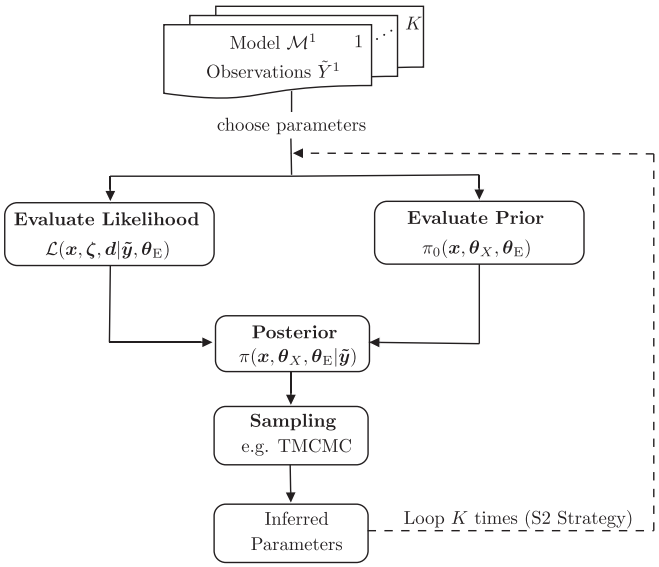


**Fig. 1.** The proposed approach of PI.

$$\left(\tilde{\boldsymbol{Y}}^1,\cdots,\tilde{\boldsymbol{Y}}^K\middle|\boldsymbol{x},\boldsymbol{\xi},\boldsymbol{d}\right)\sim\pi_{\mathrm{E}}(\tilde{\boldsymbol{y}}-\mathcal{G}(\boldsymbol{x},\boldsymbol{\xi},\boldsymbol{d});\boldsymbol{\Sigma}),$$

where $\boldsymbol{\Sigma}=diag\{\boldsymbol{\Sigma}^1,\cdots,\boldsymbol{\Sigma}^K\}\in\mathbb{R}^{N\times N}$ is the global covariance matrix and $N=\sum_{k=1}^{K}n^k$. Assuming that data in each experiment are conditionally independent given the unknowns, the likelihood in Eq. (4) is updated, as follows:

$$\mathscr{L}\left(\boldsymbol{x},\boldsymbol{\xi},\boldsymbol{d}|\tilde{\boldsymbol{y}}^1,\cdots,\tilde{\boldsymbol{y}}^K,\boldsymbol{\theta}_{\mathrm{E}}\right)=\prod_{k=1}^{K}\mathscr{L}^k\left(\boldsymbol{x},\boldsymbol{\xi},\boldsymbol{d}|\tilde{\boldsymbol{y}}^k,\boldsymbol{\theta}_{\mathrm{E}}^k\right),\tag{8}$$

where $\mathscr{L}^k(\boldsymbol{x},\boldsymbol{\xi},\boldsymbol{d}|\tilde{\boldsymbol{y}}^k,\boldsymbol{\theta}_{\mathrm{E}}^k)=\prod_{i=1}^{n^k}\pi_{\mathrm{E}}(\tilde{\boldsymbol{y}}_i^k-\mathscr{G}_i^k(\boldsymbol{x},\boldsymbol{\xi},\boldsymbol{d});\Sigma_i^k)$ is the likelihood of the observations of the $k^{th}$ experiment.

The posterior is written as $\pi(\boldsymbol{x},\boldsymbol{\theta}_X,\boldsymbol{\theta}_{\mathrm{E}}|\tilde{\boldsymbol{y}}^1,\cdots,\tilde{\boldsymbol{y}}^K)\propto\pi(\tilde{\boldsymbol{y}}^1,\cdots,\tilde{\boldsymbol{y}}^K|\boldsymbol{x})\cdot\pi_0(\boldsymbol{x},\boldsymbol{\theta}_X,\boldsymbol{\theta}_{\mathrm{E}})$. It can be evaluated as normal using (for example) the TMCMC algorithm or any other appropriate method.

### 3.2. Strategy 2 (S2)

In the stochastic UQ framework utilized in the PI process, the concept of sensitivity plays a key role in finding unknowns. The more the given model is sensitive to the unknown parameter, the lower is the uncertainty of this inferred parameter. In this sense, an adapted sequential Bayesian approach is built, named the *sensitivity-based* strategy (S2), to achieve the goal of increasing the quality of the identified parameters.

The observations $\tilde{\boldsymbol{y}}$ are classified into $K$ subsets, based on the sensitivity of the unknown parameters, that is, $\tilde{\boldsymbol{y}}=\{\tilde{\boldsymbol{y}}^1,\cdots,\tilde{\boldsymbol{y}}^K\}^T$ of the forward model $\mathscr{M}$ of the considered system. Then, the Bayesian updating framework is sequentially applied in a step-wise manner associated with the obtained subsets, by assuming the mutual independence of the observation subsets, in other words, $\pi(\tilde{\boldsymbol{y}}^1,\cdots,\tilde{\boldsymbol{y}}^K)=\prod_{k=1}^{K}\pi(\tilde{\boldsymbol{y}}^k)$.

In the first step at $k=1$, the joint prior $\pi_0(\boldsymbol{x},\boldsymbol{\theta}_X,\boldsymbol{\theta}_{\mathrm{E}})$ and the first set of observations $\tilde{\boldsymbol{y}}^1$ are utilized to build the posterior, as follows:

$$\pi^1\left(\boldsymbol{x},\boldsymbol{\theta}_X,\boldsymbol{\theta}_{\mathrm{E}}\middle|\tilde{\boldsymbol{y}}^1\right)=\frac{\mathscr{L}^1(\boldsymbol{x},\boldsymbol{\xi},\boldsymbol{d}|\tilde{\boldsymbol{y}}^1)\cdot\pi_0(\boldsymbol{x},\boldsymbol{\theta}_X,\boldsymbol{\theta}_{\mathrm{E}})}{\pi(\tilde{\boldsymbol{y}}^1)}.\tag{9}$$

In the following steps, the posterior of the previous step $\pi(\boldsymbol{x},\boldsymbol{\theta}_X,\boldsymbol{\theta}_{\mathrm{E}}|\tilde{\boldsymbol{y}}^1)$ and the corresponding set of observations $\tilde{\boldsymbol{y}}^k$ are used, until the end of the observations subsets is reached, that is, $k=2,\cdots,K$. The posterior of the step $k^{th}$ could then be generalized to

$$\pi^k\left(\boldsymbol{x},\boldsymbol{\theta}_X,\boldsymbol{\theta}_{\mathrm{E}}\middle|\tilde{\boldsymbol{y}}^1,\cdots,\tilde{\boldsymbol{y}}^k\right)=\frac{\mathscr{L}^k(\boldsymbol{x},\boldsymbol{\xi},\boldsymbol{d}|\tilde{\boldsymbol{y}}^k)\cdot\pi^{k-1}(\boldsymbol{x},\boldsymbol{\theta}_X,\boldsymbol{\theta}_{\mathrm{E}}|\tilde{\boldsymbol{y}}^{k-1})}{\pi(\tilde{\boldsymbol{y}}^k)}.\tag{10}$$

In each step, the parameters are inferred by implementing the MCMC method, namely, the TMCMC algorithm. However, this increases the computational time of the whole process because the parameters are inferred at each sub-step. At the same time, it is still reasonable and has significant advantages in improving the convergence of the MCMC algorithm and enhancing the quality of the identified parameters.

## 4. Case study

### 4.1. Introduction

The case study utilizes the catenary poles installed along the high-speed train track between Erfurt and Halle/Leipzig in Germany. The case study provides a unique opportunity to analyze a newly-built structure at different stages: production, installation, and service life. To achieve this, a short-term experimental program and a long-term monitoring system were developed to collect the statistical data of the real system. The experimental program was implemented in the laboratory through a series of short-term tests to verify the properties of the spun-cast poles. This included (but was not limited to) the verification of geometry, vibration tests, and 3-point bending test. More details about this program are available in Ref. [46]. However, the tests used in this study are described in detail in Section 4.3.

### 4.2. Geometry and materials

The studied structure is 10 m in height with tapered hollow circular sections. The outer diameter at the bottom end is 400 mm and reduces linearly to 250 mm at the top of the pole. The pole is produced by a spinning method. The geometric of the spun-cast pole is summarized in Table 1.

Nominal material properties of the structure were extracted from the datasheet and are summarized in Table 2.

### 4.3. Experimental program

#### 4.3.1. Vibration test

A pole was tested in a vibration test in free-free setup by hanging it in a horizontal position using two ropes, as shown in Fig. 2. A set of twelve 1D accelerometers (type PCB Peizotronics 393A03) were attached to the pole to measure the accelerations in the horizontal and vertical directions, according to the test setup. Two of the sensors were fixed to the

**Table 1**
The nominal geometry of the poles.

| Dimension | Nominal value |
|---|---|
| Length, $L$ [m] | 10 |
| Outer diameter at the bottom, $d_{bot}$ [mm] | 400 |
| Outer diameter at the top, $d_{top}$ [mm] | 250 |
| Wall thickness at the bottom, $t_{bot}$ [mm] | 62 |
| Wall thickness at the top, $t_{top}$ [mm] | 52 |

**Table 2**
The nominal material properties of the poles.

| Material | Value |
|---|---|
| **Concrete** | |
| Concrete grade | C80/95 |
| **Prestressing** | |
| Prestressing strands | 7/16″ St 1680/1880 |
| Number of strands, $n_{st}$ | 10 |
| Area of the strand, $A_{st}$ [mm$^2$] | 70 |
| Initial prestressing stress, $\sigma_{PT}$ [MPa] | 975 |

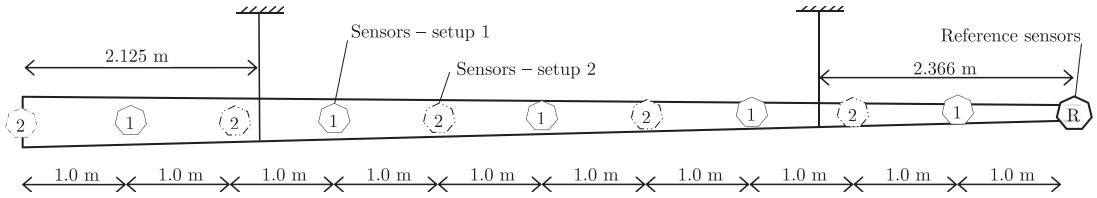


**Fig. 2.** The vibration test of the pole – schematic experimental setup.

top end of the pole, and considered as reference sensors while the rest were configured in two measurement setups to increase the quantity and quality of the identified mode shapes and natural frequencies.

Moreover, a hammer with an appropriate hardness of impact tip was used to excite the structure in three positions in both horizontal and vertical directions. The procedure was repeated for each sensor-setup. In the first sensor-setup, the sensors were attached with an in-between distance of 2.0 m. Then, these sensors were moved 1.0 m toward the bottom of the pole to form the second measuring setup, as shown in Fig. 2.

Data was acquired at a sampling rate of 4096 Hz. The modal parameters were identified using the recorded accelerations from the two setups. The data were analyzed using the Operational Modal Analysis (OMA), based on the output-only data [47]. The covariance-driven version of the Stochastic Subspace Identification (SSI) method [48] was implemented to compute the covariances of the identified system and modal parameters using the MACEC toolbox [49] (for further reading about SSI, refer to Ref. [50]). The modal parameters of the first five modes in both horizontal and vertical directions were identified. The results of the SSI analysis are shown in Fig. 3 for vertical direction. The identified natural frequencies **f** and the damping ratios ζ are listed in Table 3.

#### 4.3.2. 3-Point bending test

Later, the same pole was tested in a 3-point bending setup. The pole was tested horizontally in a simply-supported setup. The supports were made to fit the circular shape of the pole. The pole was supported at1.5 m from each of the ends, resulting in a mid-span of7 m. The schematic experiment setup is shown in detail in Fig. 4. The pre-specified displacements were applied vertically at mid-span in steps by a servo-hydraulic piston, until the failure of the pole, as shown in Fig. 5.

During the test, deflection of the pole was recorded continuously, using Inductive Displacement Transducers (IDT) in three positions, P1, P2, and P3, as shown in Fig. 4. The maximum load was 81 kN corresponding to deflection of 110 mm, 63 mm, 71 mm at the points P1, P2, and P3, respectively (see the dash-dotted lines in Fig. 10). It was evident that the measured loads and deflections were more than those calculated from the preliminary analysis by approximately 20%. These increments are ascribed to the differences between the '*real*' properties of the structure and the nominal values mentioned in the datasheet. These differences indicate the importance of identifying the real geometry and material properties before evaluating the actual behavior of the structure.

For greater understanding and in-depth verification of the nature of the structure and the ongoing test, a deflection-wise sensitivity analysis is accomplished. This analysis is fundamental to this study as it shows the most dominant parameters at each step of the test. In this analysis, we discretize the envelope of the load-deflection hysteresis curve and implement a sensitivity analysis. As a result, Sobol sensitivity indices [51, 52], based on the variance method at each discretization point, are calculated.

The results of the sensitivity analysis at P1 are shown in Fig. 6. As a conclusion, the modulus of elasticity $E_c$ is dominant in the first part of the test up to a deflection of 6 mm. For the deflection values between 6 and 80 mm, both the concrete tensile strength $f_{ctm}$ and the prestressing initial strain $\varepsilon_{PT}$ are the leading parameters. For the remainder, until the failure point is reached, the compression strength of the concrete $f_{cm}$ and the concrete strain at maximum compressive stress, $\varepsilon_c$ become the most critical parameter.

### 4.4. Modeling

#### 4.4.1. Theoretical background

The vertical displacement under the forced lateral vibration of a non-uniform beam can be described by the general equation of motion [53] that describes the behavior of the given structure under the conducted experiments

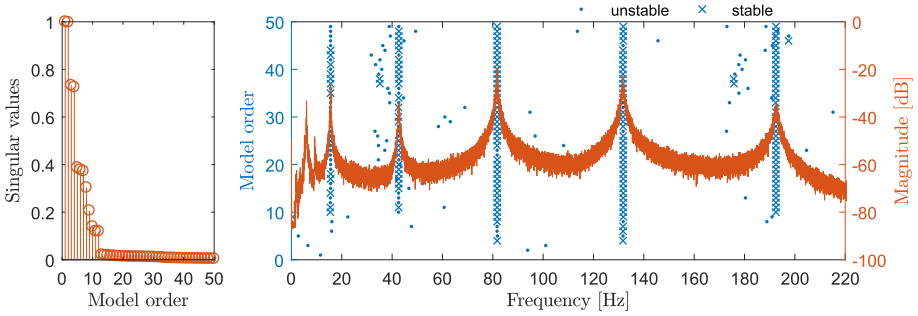


**Fig. 3.** The results of the SSI analysis of the pole in the vertical direction: the singular values of the output covariance matrix (left), and the stabilization diagram (right).

**Table 3**
The Natural frequencies **f** and the damping ratios ζ of the first five mode shapes of the un-damaged pole [46].

| Mode shape[a] | 1 - v | 2 - v | 3 - v | 4 - v | 5 - v | 1 - h | 2 - h | 3 - h | 4 - h | 5 - h |
|---|---|---|---|---|---|---|---|---|---|---|
| **f**[Hz] | 15.56 | 42.67 | 81.72 | 131.69 | 192.43 | 15.56 | 42.17 | 81.09 | 131.58 | 192.68 |
| ζ [%] | 0.87 | 0.72 | 0.28 | 0.38 | 0.47 | 0.33 | 0.33 | 0.36 | 0.26 | 0.81 |

[a] $(i-\mathrm{v}), (i-\mathrm{h})$ are the $i^{th}$ mode shape in vertical and horizontal directions, respectively, $i = 1, \cdots, 5$.

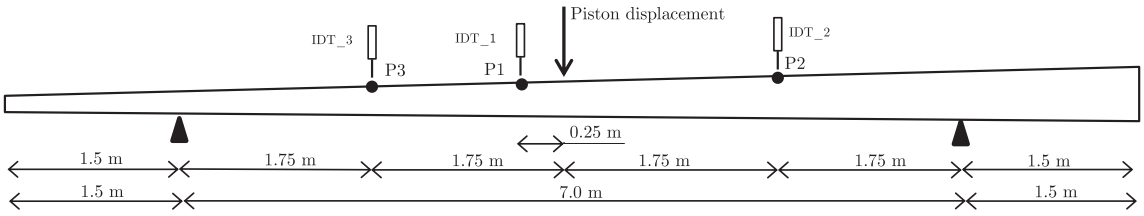


**Fig. 4.** 3-point bending test – schematic experimental setup.

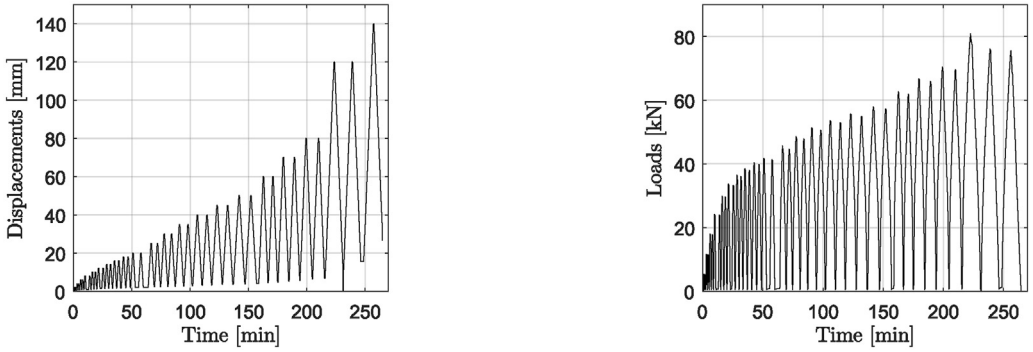


**Fig. 5.** The applied loading regime of the 3-point bending test: the applied displacements at the mid-span (left), and the corresponding piston loads (right).

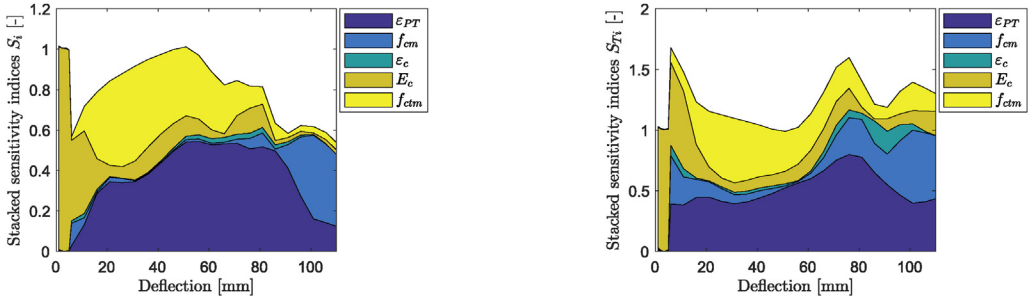


**Fig. 6.** Stacked sensitivity indices at the point P1: first-order sensitivity indices $S_i$ (left), and total effects sensitivity indices $S_{Ti}$ (right).

$$\frac{\partial^2}{\partial x^2}\left[EI(x)\frac{\partial^2 w}{\partial x^2}(x,t)\right]+\rho A(x)\ \frac{\partial^2 w}{\partial t^2}(x,t)=f(x,t)\ , \tag{11}$$

where $E$ is equivalent young's modulus of the section; $I(x)$ is second moment of inertia of the cross-section of the beam about the horizontal axis. ρ is the equivalent mass density, and $A(x)$ is the cross-sectional area. $w$ denotes the vertical displacement under the external force per unit length $f(x,t)$. $x$ is the axial coordination of the beam, and $t$ represents the time.

Based on Eq. (11) the natural frequencies of the structure together with the corresponding mode shapes can be determined. The common analytical solution of the selected structure is given, as follows:

$$\mathbf{f}_i=\frac{\lambda_i^2}{2\pi L^2}\sqrt{\frac{EI_{bot}}{\rho A_{bot}}},\ i=1,2,3,\cdots, \tag{12}$$

where $\mathbf{f}_i$ is the natural frequency corresponding to the $i^{th}$ mode shape, $\lambda_i$ is a constant; $L$ is the length of the beam. The terms $I_{bot}$ and $A_{bot}$ denote the moment of inertia of the cross-section at the bottom of the pole, and the cross-sectional area at the bottom of the pole, respectively [54]. In addition, the bending behavior of the beam is well studied and described in the literature (see, for example [53]) and can be well calculated by Eq. (11).

#### 4.4.2. Numerical model

A fully-detailed FEM model to simulate each of the experimental tests was built. The concrete material was simulated using volume elements with eight nodes, each with three degrees of freedom. The sizes of volume elements were approximately 50 × 50 × 25 mm in the longitudinal, circumferential, and radial directions, respectively. Further, the prestressing strands were simulated using 3D truss elements with two nodes and three degrees of freedom at each node.

The concrete constitutive model was carefully built to match the linear and nonlinear behavior of the concrete. The selected model covers both softening and hardening behavior of the concrete in tension and compression, respectively. The selected model covers two main failure mechanisms: tensile cracking, and compressive crushing. Moreover, the selected concrete constitutive model has the advantage of simulating material in the post-cracking phase, which is mainly required for the simulation pole in the 3-point bending test [55].

The stress-strain curves of concrete in compression and tension were derived from the Fib Model Code 2010 [56]. The concrete in compression follows a parabolic curve until the material attains $f_{cm}$ corresponding to a strain of $\varepsilon_c$. Then, it is followed by strain softening until the concrete reaches a crushing strain $\varepsilon_{cu}$ of 3.1‰. The behavior of concrete in tension is considered linear until the mean tensile strength of concrete $f_{ctm}$ is reached. Then, it reduces linearly to the maximum tensile strain of the concrete. The constitutive model of the steel follows the elastic-plastic behavior to demonstrate the expected behavior during the 3-point bending test.

To accelerate the different analyses in this study, surrogate models to overcome the heavy computations of the numerical models were used. non-parametric regression models were built, based on the Kriging method [57]. To assure that the surrogate models matched the numerical models to an acceptable tolerance, the Root Mean Squared Error (RMSE), the Coefficient of Determination (CoD), and the Predicted Coefficient of Determination (PoD) of different models were calculated.

## 5. Application

### 5.1. General considerations

The flow chart in Fig. 7 depicts the implementation of the proposed approach to infer the unknown parameters $\boldsymbol{x}$ of the given case study using the available observations $\tilde{\boldsymbol{y}}$. This is achieved based on three tracks (T1, T2, and T3) that are shown in Table 4. In the tracks T1 and T2, the proposed strategies (S1 and S2) are applied, in parallel, using the observations of the 3-point bending test of the pole. Then, the most relevant results of one of the applied strategies are consequently chosen. In track T3, some of the identified parameters are selected as informative priors for the PI process, using the observations of the vibrations test and strategy S1.

For the sake of this study, the geometry parameters, the properties of the reinforcement bars, and the prestressing stands were considered as deterministic parameters $\boldsymbol{d}$. The geometry of the corresponding model $\mathscr{M}$ is built, based on the nominal values that are shown in Table 1. The exceptions are the thicknesses of the walls where the measured values from the laboratory are applied. The nominal properties of the prestressing and the reinforcement steel are applied as listed in Table 2.

From the UQ framework and the engineering point of view, the key parameters that have a significant influence on the behavior of the pole are the concrete properties and the strains of the prestressing strands. For this reason, the vector of the unknown parameters is $\boldsymbol{x} \equiv \{\varepsilon_{PT}, f_{cm}, \varepsilon_c, f_{ctm}, E_c, \rho_c\}^T$.

Except for the prestressing initial strain $\varepsilon_{PT}$, the prior densities of the unknown parameters $\boldsymbol{x}$ are assigned to follow PDFs of uniform distributions. This is because the prior knowledge of parameters is not enough to formulate informative priors. The priors $\pi_0(\boldsymbol{x})$ are carefully bounded, based on the available information and engineering prejudgment considering the values recommended by fib Model Code 2010 [56], that is, $\pi_0(\boldsymbol{x})\,\widetilde{\mathscr{U}}(a,b)$, as listed in Table 5.

Based on the measurements (see Section 4.3.2), the prior distribution of $\varepsilon_{PT}$ follows a normal distribution $\pi_0(\varepsilon_{PT})\widetilde{\mathscr{N}}(\mu_{PT}, \sigma^2_{PT})$ with unknown mean $\mu_{PT}$ and variance $\sigma^2_{PT}$. In this case, the literature recommends considering the conjugate priors of the hyperparameters $\boldsymbol{\theta}_x$ as the normal distribution for the unknown mean and the inverse gamma distribution for the unknown variance [29]. Accordingly, the priors of the mean $\mu_{PT}$ and the variance $\sigma^2_{PT}$ are chosen, such as $\pi_0(\mu_{PT})\widetilde{\mathscr{N}}(3.1, 0.4)$ and $\pi_0(\sigma^2_{PT})\widetilde{\mathscr{IG}}(5.0, 0.126)$, respectively. This corresponds with a maximum *a Priori* $MAPr_{\sigma^2_{PT}} = 0.021$ and a standard deviation $SD_{\sigma^2_{PT}} = 0.018$. Besides, the variance of the total errors $\sigma^2_{\mathrm{E}}$ is chosen to be a global hyperparameter $\theta_{\mathrm{E}}$ has a uniform prior distribution $\pi_0(\sigma_{\mathrm{E}})\,\widetilde{\mathscr{U}}(0.005,\ 0.1)$, which makes sense in this case. Moreover, due to some physical interpretations, the independency between the parameters was assumed.

The errors $\mathbf{E}$ is selected to have a multivariate Gaussian distribution $\mathbf{E}\widetilde{\mathscr{N}}(0, \boldsymbol{\Sigma})$ with zero-means $\mathbb{E}(\boldsymbol{\eta}) = 0$. $\boldsymbol{\Sigma}$ represents the symmetric, and positive-semidefinite covariance matrix that is unknown (at least in this case), and is estimated through the applied framework. For uncorrelated errors, the covariance matrix becomes $\boldsymbol{\Sigma} = \sigma^2_{\mathrm{E}}\ diag\{\tilde{y}_1, \cdots, \tilde{y}_n\}^2 \in \mathbb{R}^{n\times n}$, where $\sigma^2_{\mathrm{E}}$ is the variance of the errors $\boldsymbol{\eta}$.

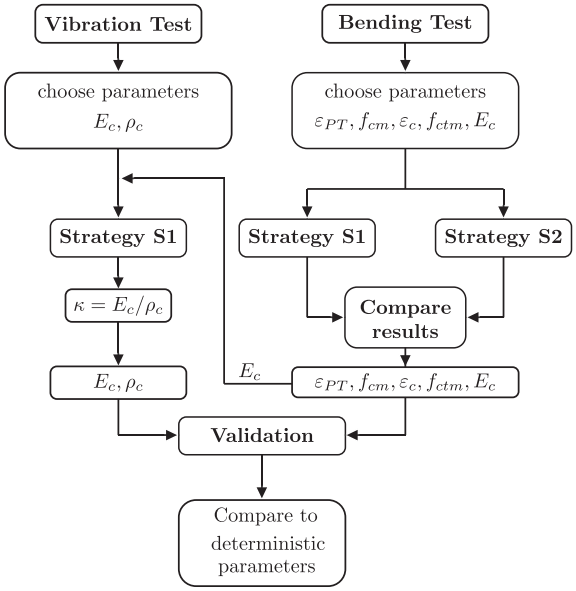


**Fig. 7.** Implementation of the proposed strategies of PI.

**Table 4**
The applied tracks.

| Track | Observations | Strategy | Identified parameters |
|---|---|---|---|
| T1 | Bending test | S1 | $\varepsilon_{PT}, f_{cm}, \varepsilon_c, f_{ctm}, E_c$ |
| T2 | Bending test | S2 | $\varepsilon_{PT}, f_{cm}, \varepsilon_c, f_{ctm}, E_c$ |
| T3 | Vibration test | S1 | $E_c, \rho_c$ |

### 5.2. Tracks T1 and T2 (bending test)

The proposed strategies S1 and S2 are implemented in parallel. Then, the results of different applied strategies are compared to detect their respective advantages. Two criteria measure the quality of the inferred parameters: the uncertainty represented by the variance of the parameters, and the shape of the posterior distribution. The realizations of the observations $\tilde{y}_i \equiv \delta_i$ are created from the deflections $\delta_i$ of the pole at different time steps at the specified point P1, P2, and P3, see Section 4.3.2.

Strategy S1 is applied by calculating the likelihood from Eq. (4) using the observation $\tilde{\boldsymbol{y}}$. To apply strategy S2, the observations are divided into three subsets, based on the sensitivity indices derived in Section 4.3.2, such that $K = 3$ and $\tilde{\boldsymbol{y}} = \{\tilde{\boldsymbol{y}}^1, \tilde{\boldsymbol{y}}^2, \tilde{\boldsymbol{y}}^3\}^T$. The corresponding deflection ranges of the subsets are specified in Table 6. In this step, the unknown

**Table 5**
The uninformative priors of the parameters.

| Parameter | PDFs |
|---|---|
| Concrete compressive strength, $f_{cm}$[MPa] | $\mathscr{U}(80, 120)$ |
| Concrete strain at maximum compressive stress, $\varepsilon_c$[‰] | $\mathscr{U}(2.5, 3.0)$ |
| Concrete tensile strength, $f_{ctm}$[MPa] | $\mathscr{U}(4.0, 6.0)$ |
| Concrete Modulus of Elasticity, $E_c$[GPa] | $\mathscr{U}(43, 53)$ |
| Concrete density, $\rho_c$[gcm$^{-3}$] | $\mathscr{U}(2.1, 2.5)$ |

**Table 6**
The classification of the observations $\tilde{\boldsymbol{y}}$ (strategy S2). The deflection at mid-span (Point P1) as a reference.

| Step | Observation subset | Deflection range [ mm] | Sensitive parameters |
|---|---|---|---|
| 1 | $\tilde{\boldsymbol{y}}^1$ | [0–6] | $E_c$ |
| 2 | $\tilde{\boldsymbol{y}}^2$ | (6–80] | $f_{ctm}, \varepsilon_{PT}$ |
| 3 | $\tilde{\boldsymbol{y}}^3$ | (80–110] | $f_{cm}, \varepsilon_c$ |

parameters vector $\boldsymbol{x} \equiv \{\varepsilon_{PT}, f_{cm}, \varepsilon_c, f_{ctm}, E_c\}^T$ are inferred, where the concrete density $\rho_c$ cannot be identified in this step due to the nature of the measurements.

At the end of the tracks T1 and T2, the unknown parameters are estimated by sampling from the posterior $\pi(\mu_{PT}, \sigma^2_{PT}, f_{cm}, \varepsilon_c, f_{ctm}, E_c, \sigma^2_{\mathrm{E}}|\boldsymbol{\delta})$. For this reason, the TMCMC algorithm is run for $N_s = 5 \cdot 10^3$ samples. Then, the statistical moments of the inferred parameters are calculated.

### 5.3. Track T3 (vibration test)

In this track, strategy S1 is applied by using the observations vector $\tilde{\boldsymbol{y}}$ consisting of the natural frequencies that are derived in Section 4.3.1, that is, $\tilde{y}_i \equiv \mathbf{f}_i$. Two parameters can be identified through this track corresponding to the linear behavior of the structure in the vibration test, namely, $\boldsymbol{x} \equiv \{E_c, \rho_c\}^T$.

From Eq. (12), it can be seen that $\mathbf{f}_i \propto \sqrt{E_c/\rho_c}$. This means that only the fixed ratio $\kappa = E_c/\rho_c$ can be identified. The values of $E_c$ and $\rho_c$ are unidentifiable, because any values of $E_c$ and $\rho_c$ that satisfy $\kappa$ is valid as a solution. To overcome this, the posterior of $E_c$ from track T2 is used as an informative prior in this track, because it revealed better results. This makes $\rho_c$ identifiable and results in obtaining the posteriors of $E_c$ and $\rho_c$. In this track, $5 \cdot 10^3$ samples are drawn from the posterior $\pi(E_c, \rho_c, \sigma^2_{\mathrm{E}}|\mathbf{f})$ using the TMCMC algorithm.

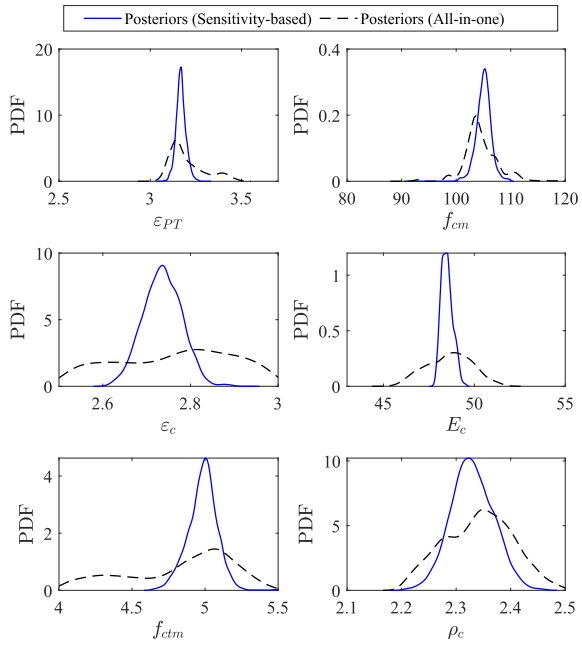


**Fig. 8.** Comparing the results of the applied Bayesian approaches: the *sensitivity-based* approach and the *All-in-one* approach.

## 6. Results and discussion

The results of tracks T1 to T3 are depicted in Fig. 8. The proposed *sensitivity-based* strategy adds significant improvements to the quality of the inferred parameters leading to more accurate posteriors with smaller variances. This is because the *sensitivity-based* S2 strategy is built in a stepwise manner. In each step, it focuses on inferring highly sensitive parameters, which leads to an increase in the quality of inferred parameters. Moreover, the obtained posteriors of these sensitive parameters are used in the following step as a formative prior, which also leads to an improvement in the quality of the other parameters. On the contrary, in the *All-in-one* S1 strategy, the sensitivity of the parameters is averaged on the full set of data, which results in losing some information that is embedded in the available observations. This results in inferring parameters at a lower quality. This emphasizes that uncertainty and sensitivity are associated, as mentioned in Section 3.2.

However, the mean values of unknown parameters are inferred by both strategies with good agreement. A summary of the statistical properties of parameters is listed in Tables 7 and 8. It is clear, how much these values differ from the nominal properties that are provided in the datasheet of the structure. The inferred parameters are 20% higher than the nominal values (see Section 4.2). This shows the importance of the PI process as an essential step before evaluating the behavior of the structure.

Correlations of different pairs of parameters are verified by the scatter plots of the samples. Fig. 9 (left) shows the high negative correlation of parameters $\varepsilon_{PT}$ and $f_{ctm}$ in the model of the 3-point bending test. These two parameters are correlated with a linear Pearson coefficient of correlation $\rho_{\varepsilon_{PT} f_{ctm}} = -0.87$. From an engineering point of view, this is correct, as the higher the applied prestressing strain $\varepsilon_{PT}$, the lower is the required tensile strength of the concrete $f_{ctm}$ to have the same cracking moment of the given cross section.

According to the results of track T3, the parameters $E_c$ and $\rho_c$ are highly correlated with a correlation coefficient of $\rho_{E_c,\rho_c} = 0.9$, as shown in Fig. 9 (right). This result is expected, as discussed in Sections 4.3.1 and 5.3. However, it supports the findings of this work. In addition, the listed hyperparameters in Table 9 are sampled from the posterior. Among these hyperparameters, $\sigma_{\mathrm{E}}$ evaluates the total errors $\boldsymbol{\eta}$ of the PI process. The inferred MAP values of the $\sigma_{\mathrm{E}}$ are 0.034 and 0.041 for the observations of bending and vibration tests, respectively, which are reasonable for the types of experiments implemented, and the numerical models.

**Table 7**
The properties of the posteriors of the identified parameters using the Bayesian strategy S1: the Maximum A Posteriori MAP, the mean value μ, and the standard deviation *SD*.

| Parameter | $\varepsilon_{PT}$ [‰] | $f_{cm}$ [MPa] | $\varepsilon_c$ [‰] | $E_c$ [MPa] | $f_{ctm}$ [GPa] | $\rho_c$ [gcm$^{-3}$] |
|---|---|---|---|---|---|---|
| MAP | 3.16 | 103.11 | 2.87 | 48.29 | 5.01 | 2.32 |
| μ | 3.20 | 104.63 | 2.76 | 48.63 | 4.83 | 2.34 |
| *SD* | 0.10 | 3.20 | 0.13 | 1.25 | 0.36 | 0.06 |

**Table 8**
The properties of the posteriors of the identified parameters using the Bayesian strategy S2: the Maximum A Posteriori MAP, the mean value μ, and the standard deviation *SD*.

| Parameter | $\varepsilon_{PT}$ [‰] | $f_{cm}$ [MPa] | $\varepsilon_c$ [‰] | $E_c$ [MPa] | $f_{ctm}$ [GPa] | $\rho_c$ [gcm$^{-3}$] |
|---|---|---|---|---|---|---|
| MAP | 3.16 | 105.36 | 2.73 | 48.06 | 5.11 | 2.32 |
| μ | 3.17 | 105.10 | 2.74 | 48.49 | 4.98 | 2.33 |
| *SD* | 0.03 | 1.36 | 0.04 | 0.32 | 0.11 | 0.04 |

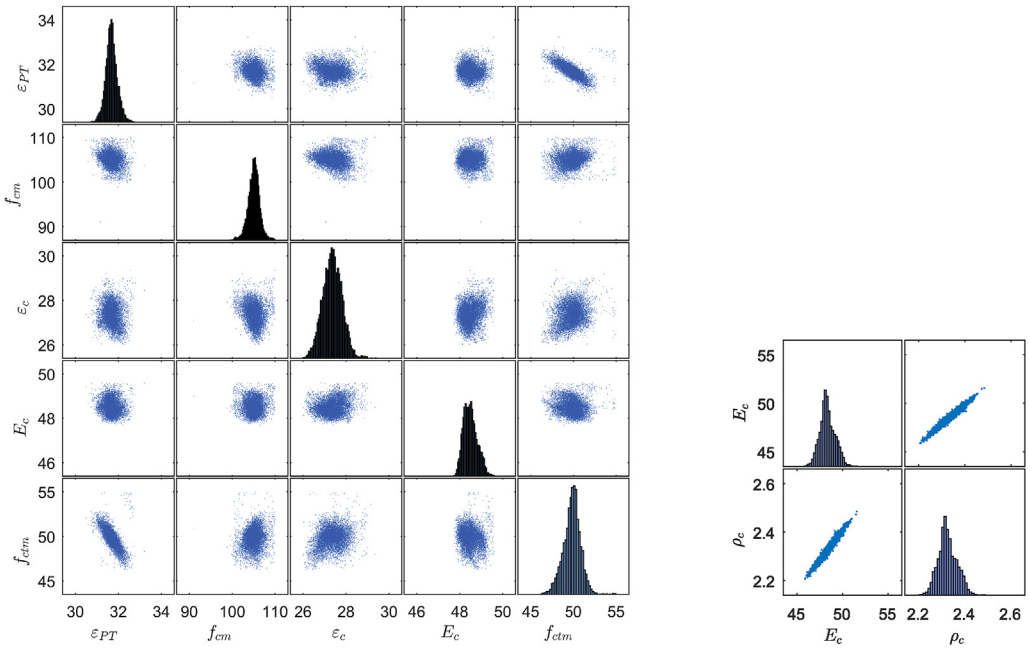


**Fig. 9.** The correlations of the identified parameters: tracks T1 and T2 using the 3-point bending test (left), track T3 using the vibration test (right).

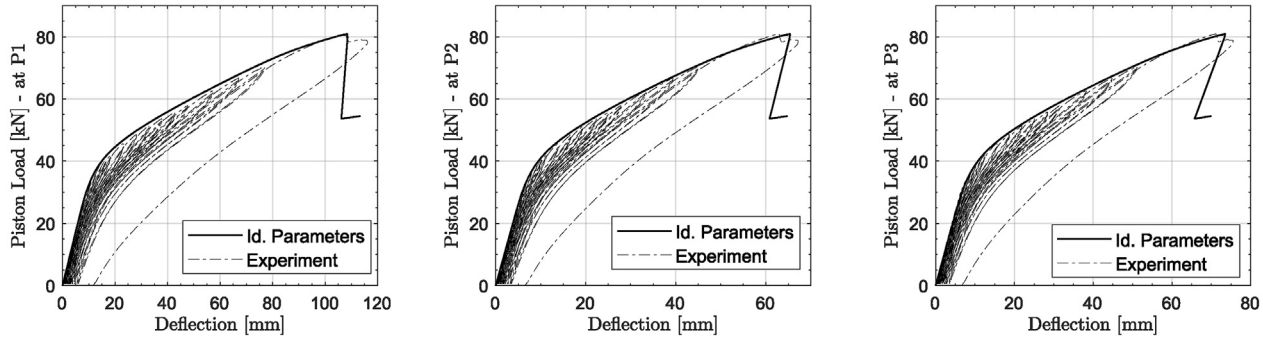


**Fig. 10.** Validation of the results using mean values of the identified parameters and the bending test model. The deflections are presented at the points P1 (left), P2 (middle), and P3 (right).

**Table 9**
The properties of the posteriors of the hyperparameters: the *Maximum A Posteriori* MAP, the mean value μ, and the standard deviation *SD*.

| Hyperparameter | $\sigma_E$[-][a] | $\sigma_E$[-][b] | $\mu_{PT}$[‰][b] | $\sigma^2_{PT}$[-][b] |
|---|---|---|---|---|
| MAP | 0.041 | 0.034 | 2.72 | 0.015 |
| μ | 0.040 | 0.029 | 2.86 | 0.023 |
| *SD* | 0.0067 | 0.0037 | 0.18 | 0.007 |

[a,b] Using the observations of vibration and bending test, respectively.

## 7. Validation of results

To validate the identified parameters, the mean values of the identified parameters from strategy S2 are used as the FEM model inputs. However, the results of the FEM are compared with the corresponding observations.

In the case of the bending test, the results of the FEM model are plotted against the hysteresis loops of the force-deflection derived from the measurements of the bending test. Fig. 10 depicts agreement between the experimental measurements of the bending test at points P1, P2, and P3, together with the outputs of the FEM model.

In the same manner, the first five natural frequencies in the horizontal and vertical direction (according to the test setup) are derived from the FEM model using the inferred parameters. The results are listed in Table 10. The trivial differences show that the results of the FEM model conform (with high accuracy) with the experimental observations of the vibration test.

Finally, the inferred parameters are verified by comparing them with conventional values of the concrete properties that are specified by the different engineering standards. Accordingly, the equations of the Fib Model Code 2010 [56], which specifies the concrete properties based on the compressive strength of the concrete $f_{cm}$, are utilized. Thus, the MAP values of the $f_{cm}$ from Table 8 are used. The calculated properties show

**Table 10**
Validation of the results - vibration test, based on the identified parameters through the *'sensitivity-based'* Bayesian approach. The natural frequencies listed in Table 3 are used as reference.

| Mode shape [a] | 1 - v | 2 - v | 3 - v | 4 - v | 5 - v | 1 - h | 2 - h | 3 - h | 4 - h | 5 - h |
|---|---|---|---|---|---|---|---|---|---|---|
| **f** [Hz] | 15.54 | 42.09 | 81.16 | 131.76 | 192.83 | 15.37 | 41.65 | 80.35 | 130.48 | 191.04 |
| Difference [%] | 0.13 | 1.36 | 0.69 | 0.05 | 0.21 | 1.22 | 1.23 | 0.92 | 0.84 | 0.85 |

[a] $(i-\mathrm{v}), (i-\mathrm{h})$ are the $i^{th}$ mode shape in vertical and horizontal directions, respectively, $i = 1, \cdots, 5$.

**Table 11**
The concrete properties based on the recommendation of the Fib code [56] and the MAP of the $f_{cm} = 105.36$ MPa. The MAP values listed in Table 3 are used as reference.

| Parameter | $f_{cm}$ [MPa] | $\varepsilon_c$ [‰] | $E_c$ [MPa] | $f_{ctm}$ [GPa] |
|---|---|---|---|---|
| value | 105.36 | 2.90 | 47.10 | 5.18 |
| Difference [%] | – | 6.20 | 3.10 | 1.40 |

that the inferred parameters are in line with the recommended values of the given code with relatively acceptable tolerance, as shown by the differences in Table 11.

## 8. Conclusion

The Bayesian probabilistic approach was applied to identify unknown parameters of the given structure. First, the empirical Bayesian approach was implemented through the *All-in-one* strategy (S1), where six parameters were inferred by utilizing the FEM model and observations of the multiple experiments.

To improve the quality of inferred parameters, an adapted sequential Bayesian approach was proposed. This approach was implemented through the *sensitivity-based* strategy (S2) by dividing the observations into subsets based on the sensitivity of the parameters. Then, the Bayesian approach was applied in a sequential manner, considering the posterior of the current step as prior to the subsequent step.

In both strategies, the TMCMC algorithm was used to sample from the posterior. The results showed a considerable improvement in the quality of the inferred parameters and confirmed the associations between the uncertainty and the sensitivity of the parameters. Furthermore, considering the unknown total errors as hyperparameters allowed to evaluate the total errors of the whole PI process.

In the validation step, a perfect agreement was achieved when using the mean values of the inferred parameters as inputs for the numerical model to compare results to the experimental observations. Additionally, it is proved that the inferred properties of the concrete were in line with the recommended values of the Fib Model Code 2010 for the same compressive strength. It has to be noted that the determined concrete compressive strength increased considerably concerning the values used in design due to the use of high strength concrete and the ongoing hardening process after the normative compressive strength at the age of 28 days, which is mandatory for the design.

The considerable deviation between the inferred parameters and the nominal ones drew attention to the importance of the PI process before conducting any study on the existing structures. This emphasized the argument at the beginning of this paper and laid the foundations for a more appropriate implementation of the subsequent phases of this study. Furthermore, applying the proposed approach looks very promising to similar applied case studies and systems that have time-dependent measurements.

## Acknowledgment

This work was done under the support of the Deutsche Forschungsgemeinschaft (DFG) through the Research Training Group 1462, which is greatly acknowledged by the authors. Another acknowledgment goes to the German Academic Exchange Service (DAAD) for supporting the main author through the scholarship program “Leadership for Syria”. This work was supported by the Center for Research and Development in Mathematics and Applications (CIDMA) through the Portuguese Foundation for Science and Technology (FCT - Fundação para a Ciência e a Tecnologia), references “UIDB/04106/2020 and UIDP/04106/2020”.

Appreciations should also be paid to Dr. Luise Göbel, Sebastian Rau, and Igor Kavrakov for their contribution in planning and conducting the experimental tests used in this paper.

## References

[1] J. Rodgers, E. Thomas, Prestressed concrete poles: state-of-the-art, PCI J. 29 (5) (1984) 52–103.
[2] F.H. Fouad, D. Sherman, R.J. Werner, Spun prestressed concrete poles–past, present, and future, Concr. Int. 14 (11) (1992) 25–29.
[3] C. Müller, M. Empelmann, F. Hude, T. Adam, Schleuderbetonstützen aus hochfester bewehrung und ultrahochfestem beton: anlässlich des 475-jahr-jubiläums des stahlwerks annahütte, Beton-und Stahlbetonbau 107 (10) (2012) 690–699.
[4] F.H. Fouad, R.J. Detwiler, High-strength materials for spun concrete poles, PCI J. 57 (3) (2012) 27–32.
[5] A. Fam, Development of a novel pole using spun-cast concrete inside glass-fiber-reinforced polymer tubes, PCI J. 53 (3) (2008) 100–113.
[6] G. Kouroussis, O. Verlinden, D.P. Connolly, M.C. Forde, Estimation of Railway Vehicle Speed Using Ground Vibration Measurements, 21st International Congress on Sound and Vibration (ICSV21), Beijing, China, 2014, pp. 1–8.
[7] D. Connolly, G. Kouroussis, P. Woodward, P.A. Costa, O. Verlinden, M. Forde, Field testing and analysis of high speed rail vibrations, Soil Dynam. Earthq. Eng. 67 (2014) 102–118.
[8] D. Connolly, G. Kouroussis, O. Laghrouche, C. Ho, M. Forde, Benchmarking railway vibrations–track, vehicle, ground and building effects, Construct. Build. Mater. 92 (2015) 64–81, https://doi.org/10.1016/j.conbuildmat.2014.07.042.
[9] P. Ampunant, F. Kemper, I. Mangerig, M. Feldmann, Train–induced aerodynamic pressure and its effect on noise protection walls, in: A. Cunha, E. Caetano, P. Ribeiro, G. Müller (Eds.), 9th International Conference on Structural Dynamics, EURODYN, 2014, pp. 3739–3743, 2014, 978-972-752-165-4.
[10] D. He, Q. Gao, W. Zhong, A Numerical Method Based on the Parametric Variational Principle for Simulating the Dynamic Behavior of the Pantograph-Catenary System, Shock Vib. (2018) 2018.
[11] O.V. Van, J.-P. Massat, E. Balmes, Waves, modes and properties with a major impact on dynamic pantograph-catenary interaction, J. Sound Vib. 402 (2017) 51–69.
[12] J. Pombo, J. Ambrósio, Influence of pantograph suspension characteristics on the contact quality with the catenary for high speed trains, Comput. Struct. 110 (2012) 32–42.
[13] L. Abrahamczyk, F. Alkam, A.H. Hisham, L. Göbel, Z. Jaouadi, M. Kraus, I. Kavrakov, D. Legatiuk, F. Mucha, S. Rau, GRK 1462 - reference Project “poles”: monitoring system, lab experiments and long-term measurements, in: L. Abrahamczyk, D. Legatiuk, F. Werner (Eds.), GRK 1462 International Workshop 2017. 26th - 28th April. Coupled Numerical and Experimental Models in Structural Engineering, Weimar, Germany, 2017, 978-3-95773-239-2.
[14] L. Göbel, F. Mucha, Z. Jaouadi, I. Kavrakov, D. Legatiuk, L. Abrahamczyk, M. Kraus, K. Smarsly, Monitoring the structural response of reinforced concrete poles along high-speed railway tracks, in: Proceedings International RILEM Conference on Materials, Systems and Structures in Civil Engineering–Conference Segment on Reliability, Technical University of Denmark Lyngby, Denmark, 2016, pp. 1–10.
[15] J.V. Beck, K.J. Arnold, Parameter Estimation in Engineering and Science, Wiley, New York, 1977.
[16] J.P. Hessling, Uncertainty Quantification and Model Calibration, Intech, 2017.
[17] S.O. Funtowicz, J.R. Ravetz, Uncertainty and Quality in Science for Policy, vol. 15, Springer Science & Business Media, 1990.
[18] D. Bigoni, A. Engsig-Karup, Uncertainty Quantification with Applications to Engineering Problems, DTU Compute, 2014.
[19] A. Tarantola, Inverse Problem Theory and Methods for Model Parameter Estimation, Society for Industrial and Applied Mathematics, 2005, https://doi.org/10.1137/1.9780898717921.
[20] H. Banks, A. Cintrón-Arias, F. Kappel, Parameter selection methods in inverse problem formulation, in: Mathematical Modeling and Validation in Physiology, Springer, 2013, pp. 43–73.
[21] F. Alkam, T. Lahmer, Quantifying the uncertainty of identified parameters of prestressed concrete poles using the experimental measurements and different optimization methods, Eng. Appl. Sci. 4 (4) (2019) 84–92, https://doi.org/10.11648/j.eas.20190404.13.
[22] R.C. Aster, B. Borchers, C.H. Thurber, Parameter Estimation and Inverse Problems, second ed. Edition, Academic Press, 2013, https://doi.org/10.1016/B978-0-12-385048-5.00030-6.
[23] J. Idier, Bayesian Approach to Inverse Problems, John Wiley & Sons, 2013.
[24] Y.M. Marzouk, H.N. Najm, L.A. Rahn, Stochastic spectral methods for efficient Bayesian solution of inverse problems, J. Comput. Phys. 224 (2) (2007) 560–586, https://doi.org/10.1016/j.jcp.2006.10.010.
[25] E. Simoen, C. Papadimitriou, G. Lombaert, On prediction error correlation in Bayesian model updating, J. Sound Vib. 332 (18) (2013) 4136–4152, https://doi.org/10.1016/j.jsv.2013.03.019.
[26] B. Lei, G. Xu, M. Feng, F. Van der Heijden, Y. Zou, D. de Ridder, D.M. Tax, Classification, Parameter Estimation and State Estimation: an Engineering Approach Using MATLAB, John Wiley & Sons, 2017.
[27] J. Kaipio, E. Somersalo, Statistical and Computational Inverse Problems, vol. 160, Springer Science & Business Media, 2006.
[28] D. Calvetti, E. Somersalo, An Introduction to Bayesian Scientific Computing: Ten Lectures on Subjective Computing, vol. 2, Springer Science & Business Media, 2007, https://doi.org/10.1007/978-0-387-73394-4.
[29] A. Gelman, J.B. Carlin, H.S. Stern, D.B. Rubin, Bayesian Data Analysis, third ed. Edition, vol. 2, Chapman & Hall/CRC, Boca Raton, FL, USA, 2014.
[30] J.B. Nagel, B. Sudret, A unified framework for multilevel uncertainty quantification in Bayesian inverse problems, Probabilist. Eng. Mech. 43 (2016) 68–84.
[31] A.M. Stuart, Inverse problems: a Bayesian perspective, Acta Numer. 19 (2010) 451–559.

[32] C.A.L. Bailer-Jones, Practical Bayesian Inference: A Primer for Physical Scientists, Cambridge University Press, 2017, https://doi.org/10.1017/9781108123891.
[33] J.L. Beck, L.S. Katafygiotis, Updating models and their uncertainties. I: Bayesian statistical framework, J. Eng. Mech. 124 (4) (1998) 455–461, https://doi.org/10.1061/(ASCE)0733-9399, 1998)124:4(455.
[34] C.M. Bishop, Pattern Recognition and Machine Learning (Information Science and Statistics), Springer-Verlag, Berlin, Heidelberg, 2006.
[35] W.R. Gilks, S. Richardson, D. Spiegelhalter, Markov Chain Monte Carlo in Practice, Chapman and Hall/CRC, 1995.
[36] W.K. Hastings, Monte Carlo Sampling Methods Using Markov Chains and Their Applications, 1970.
[37] S. Chib, E. Greenberg, Understanding the metropolis-hastings algorithm, Am. Statistician 49 (4) (1995) 327–335.
[38] J. Ching, Y.-C. Chen, Transitional Markov chain Monte Carlo methods for Bayesian model updating, model class selection, and model averaging, J. Eng. Mech. 133 (7) (2007) 816–832, https://doi.org/10.1061/(ASCE)0733-9399, 2007)133:7(816.
[39] P. Green, K. Worden, Bayesian and Markov chain Monte Carlo methods for identifying nonlinear systems in the presence of uncertainty, Phil. Trans. R. Soc. A 373 (2015), https://doi.org/10.1098/rsta.2014.0405, 2015) 20140405.
[40] P. Angelikopoulos, C. Papadimitriou, P. Koumoutsakos, X-TMCMC: Adaptive kriging for Bayesian inverse modeling, Comput. Methods Appl. Mech. Eng. 289 (2015) 409–428.
[41] F. Liang, C. Liu, R. Carroll, Advanced Markov Chain Monte Carlo Methods: Learning from Past Samples, vol. 714, John Wiley & Sons, 2011.
[42] P. Congdon, Bayesian Statistical Modelling, vol. 704, John Wiley & Sons, 2007.
[43] W. Betz, I. Papaioannou, D. Straub, Transitional Markov chain Monte Carlo: observations and improvements, J. Eng. Mech. 142 (5) (2016), 04016016.
[44] S.H. Cheung, J.L. Beck, Bayesian model updating using hybrid Monte Carlo simulation with application to structural dynamic models with many uncertain parameters, J. Eng. Mech. 135 (4) (2009) 243–255.
[45] J.L. Beck, S.-K. Au, Bayesian updating of structural models and reliability using Markov chain Monte Carlo simulation, J. Eng. Mech. 128 (4) (2002) 380–391.
[46] L. Göbel, F. Mucha, I. Kavrakov, L. Abrahamczyk, M. Kraus, Einfluss realer Materialeigenschaften auf numerische Modellvorhersagen: fallstudie Betonmast, Bautechnik 95 (1) (2018) 111–122, https://doi.org/10.1002/bate.201600091.
[47] R. Brincker, C.E. Ventura, Introduction to Operational Modal Analysis, John Wiley & Sons, Ltd, 2015, https://doi.org/10.1002/9781118535141.
[48] R. Brincker, P. Andersen, Understanding stochastic subspace identification, in: Proceedings of the 24th IMAC, St. Louis, Missouri, 2006, pp. 279–311.
[49] E. Reynders, M. Schevenels, G. De Roeck, Macec 3.3: A Matlab Toolbox for Experimental and Operational Modal Analysis, 2014.
[50] E. Reynders, G. De Roeck, Reference-based combined deterministic–stochastic subspace identification for experimental and operational modal analysis, Mech. Syst. Signal Process. 22 (3) (2008) 617–637, https://doi.org/10.1016/j.ymssp.2007.09.004.
[51] A. Saltelli, M. Ratto, T. Andres, F. Campolongo, J. Cariboni, D. Gatelli, M. Saisana, S. Tarantola, Global Sensitivity Analysis: the Primer, John Wiley & Sons, 2008, https://doi.org/10.1002/9780470725184.
[52] A. Saltelli, S. Tarantola, F. Campolongo, M. Ratto, Sensitivity Analysis in Practice: A Guide to Assessing Scientific Models, John Wiley & Sons, Ltd, England, 2004, https://doi.org/10.1002/0470870958.
[53] S. Rao, Mechanical Vibrations, PRENTICE HALL, 2016.
[54] R.D. Blevins, Formulas for Dynamics, Acoustics and Vibration, John Wiley & Sons, Ltd, 2015, https://doi.org/10.1002/9781119038122.
[55] M. Batikha, F. Alkam, The effect of mechanical properties of masonry on the behavior of FRP-strengthened masonry-infilled RC frame under cyclic load, Compos. Struct. 134 (2015) 513–522, https://doi.org/10.1016/j.compstruct.2015.08.105.
[56] P. Beverly, in: Fib Model Code for Concrete Structures 2010, Wiley-VCH Verlag GmbH & Co. KGaA, 2013, https://doi.org/10.1002/9783433604090.
[57] D.G. Krige, A statistical approach to some basic mine valuation problems on the witwatersrand, J. Chem. Metall. Min. Soc. S. Afr. 52 (6) (1951) 119–139, https://doi.org/10.2307/3006914.